Image Dehazing Technique Based on Sky Weight Detection and Fusion Transmission

Jung-San Lee, Yun-Yi Fan, Hsin-Yu Lee, Gah Wee Yong, Ying-Chin Chen*

Department of Information Engineering and Computer Science, Feng Chia University, Taiwan
leejs@fcu.edu.tw, a19990101152@gmail.com, kngngop@gmail.com, yonggahwee@gmail.com, ycchen.blythe@gmail.com

Abstract

Computer vision techniques are widely applied to the object detection, license plate recognition, remote sensing, and outdoor monitoring system. The performance of these applications mainly relies on the high quality of outdoor image. However, an outdoor image can be led to contrast decrease, color distortion, and unclear structure by poor weather conditions and human factors such as haze, fog, and air pollution. These issues may lower down the sharpness of a photo. Despite of the single-image dehazing is used to solve these issues, it cannot achieve a satisfactory result when the method deals with the bright scene and sky area. In this article, we aim to design an adaptive dehazing technique based on fusion transmission and sky weight detection. The sky weight detection is employed to distinguish the foreground and background, while detected results are applied to the fusion strategy to calculate deep and shallow transmissions. Thus, this can get rids of the subject of over-adjustment. Experimental results have demonstrated that the new method can outperform the latest state-of-the-art methods in terms of subjective and the objective assessments.

Keywords: Dehaze, Fog, Illumination, Dark channel, Fusion

1 Introduction

Computer vision is the research that makes the machine be able to recognize a picture. Without loss of generality, the camera and computer are the commonest ones used to simulate the machine vision via image processing. The related applications are widely applied to the object detection, license plate recognition, remote sensing, and outdoor monitoring system. The performance of these techniques mainly relies on high quality of outdoor image. However, outdoor image can be led to contrast decrease, color distortion, and unclear structure by poor weather conditions and human factors such as haze, fog, and air pollution. These issues may lower down the sharpness of a photo. As a result, people cannot observe the specific scene under outdoor monitoring system and must fail to identify license plate due to inferior consequence of multimedia technology. In order to get a clear picture, it is necessary to remove the haze from an image. Thus, dehazing is a major skill to enhance the quality of vision and obtain a high accuracy on the technique of computer vision.

The dehazing method could be classified into three categories: additional information approach [1-3], multiple-image approach [4-6], and single-image approach [7-21]. In the terms of additional information approach, a dehaze model is created from the depth of fields (DOF). The information of DOF is used to adjust the height of camera or tilt angle by user. Because the approach based on additional information mainly relies on the extra messages offered by the photographer, it is unfriendly. Regards to multiple-image approach, DOF is computed according to several images under the same scene with different weather conditions. Similarly, multiple-image approach is not agile since it is constrained by extra photos.

As to single-image approach, it is utilized to address the issue of addition resources. The image is recovered by individual heuristic priors from single image. There does not require extra information. Furthermore, the single-image dehazing is the most effective method because it adopts the optical scattering model as the renovating architecture. The process of generating haze in optical scattering model is described in Figure 1, where I^c is a hazy image, J^c is a scene radiance or haze-free image, $t(x)$ is transmission, A^c is atmospheric light, and c represents color channel RGB (R: Red, G: Green, B: Blue). A hazy image I^c is established by scene radiance J^c with the transmission $t(x)$ and slight air light A^c. In other words, the haze-free image J^c is affected by the transmission $t(x)$ and atmospheric light A^c. It is a great challenge for researcher to implement single-image dehazing mechanism since the optical algorithm is hard to design with only one image. Here, we depict the classical dehazing techniques in the category of single-image. In 2008, Tan has discovered the fact that the contrast of haze-free image is higher than that of hazy one [7]. Thus, Tan can remove the haze through adjusting the contrast value of each block from an image. Nevertheless, it might cause the block effects due to discontinuous DOF. Next, Fattal has computed the transmission map based on the reflectivity of light [8]. Unfortunately, the method of Fattal is invalid to deal with the scene under strong hazy. Later on, He et al. have proposed a strategy named dark channel prior (DCP) to accurately calculate the parameters of transmission $t(x)$ and light A^c [9]. In particular, He et al. have found out the truth that there exists a minimum intensity among RGB channels of the outdoor hazy image. This fact can help bring in a better recovery consequence, which is a milestone in the field of defogging. Although DCP could be used to layout an original-like color, the outcome might have block effects. For mitigating the block distortion, Huang et al. have adopted the median filter to construct the transmission map for preserving the edges in an

*Corresponding Author: Ying-Chin Chen; E-mail: ycchen.blythe@gmail.com
DOI: 10.53106/160792642022092305005

image [11] and determined the threshold for edges of $t(x)$ at the same time.

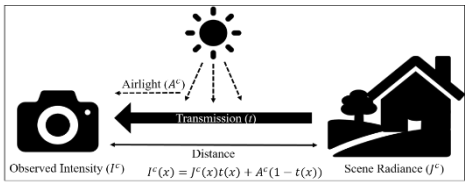

Figure 1. Optical scattering model

In addition, they tune the color of a hazy image for eliminating sandstorm. Regrettably, the scheme of Huang et al. may bring in unnatural recovered image due to discordance procedure between dehazing and de-sandstorming. To overcome the weak point of [11], Lee et al. have introduced channel-weighted analysis and employed the illumination adjustment after recovering procedure [16]. This can acquire favorable human visual perception of a photo under wild weather conditions. Nevertheless, DCP is not an appropriate dehazing strategy when illumination of scenery is similar with atmospheric light. Since the ratio of haze is low in sky region of general image, DCP is not suitable for the picture containing lots of bright, such as white architecture. Consequently, the value of illuminance and pixel shall be unbalanced if we overuse dehazing. The background might lose the real appearance in an image. The outputs of above methods are overexposure in the regions of sky and thick fog because they have employed the same intensity of transmission map [7-17]. It is not accurate enough for specific parts, including foreground and background of an image. Therefore, fusion strategy is applied to compute precise transmission for providing a better healing [18-21]. There are two classes of transmission maps in fusion strategy: strong and weak, in which the foreground and background of a photo are refined by strong $t(x)$ and weak $t(x)$, respectively. Accordingly, the whole image can be properly restored. In contrast, the refined outcome might lose the realness due to the fusion strategy ignore the focal reinforcement of an image. For mitigating this weakness, Shin et al. calculated the transmission map through statistics and analysis of reflection rate [25]. Also, Lee et al. has introduced structured guided ℓ_0-norm filter to obtain the natural dehazed image. Aside from $t(x)$, atmospheric light A is adaptively calculated [18], which can deal with the problem caused by a bright scene and make the outcome closer to the reality. On the other hands, the frameworks of machine learning are used to train the depth models with the assumption of the highest atmospheric light intensity [12-14]. However, they are only suitable for particular images. It is not flexible to deal with comprehensive applications.

In this article, we aim to design an adaptive dehazing mechanism based on fusion transmission and sky weight detection. Firstly, we classify an input by its illumination value, which can adaptively tune the procedure of recovery under different lightness. After that, sky weight detection is employed to distinguish the foreground from background. The feature of sky is estimated through a series of condition determination inspired by [20-21]. Detected results can be applied to the fusion strategy to calculate deep and shallow transmissions. This can get rids of the subject of over-adjustment. Furthermore, the proposed scheme has introduced the channel-weighted analysis [16] to refine the details and balance the irregular lightness. The experimental results have demonstrated that the new method can outperform the latest state-of-the-art methods [9-12, 15-17, 25] in terms of subjective and the objective assessments, including human perception, peak signal to noise ratio (PSNR), and structural similarity index (SSIM). The rest of this article is organized as follows. Preliminaries are introduced in section 2. The proposed mechanism is described in section 3, while the experiment results and analysis are explained in section 4. Conclusions are given in section 5.

2 Preliminary Concepts

In this section, the related schemes and the concept applied in the article are depicted. First, we explain the detail of optical scattering model, which is referred in the Introduction. The algorithm of DCP [9] on transmission map and atmospheric light is sequentially introduced. Furthermore, we describe the channel-weighted tuning [16], which is used to improve the image quality [9]. Finally, the idea of brightness map which inspires us the adoption of illumination determination is discussed [18].

A. Optical Scattering Model

The optical scattering model is used to present the information of hazy image and widely applied in dehazing technology, as illustrated in the Figure 1. The essential definitions are mentioned in the Introduction of this paper. The model is shown in Eq. (1), and the details are described as below. The first component $J(x)t(x)$ is utilized to represent direct attenuation, which explains the relationship between scene radiance and medium transmission. The second term $A(1\text{-}t(x))$ means that the process shows the color from light scattering of the scene.

$$I(x) = J(x)t(x) + A(1\text{-}t(x)) \quad \textbf{(1)}$$

Assumed that atmospheric light is homogeneous, and the transmission t can be expressed in Eq. (2) which shows that scene exponentially attenuates with the depth. It is because that transmission is related to DOF.

$$t(x) = e^{-\beta d(x)} \quad \textbf{(2)}$$

where β is the scattering coefficient of atmosphere, $d(x)$ is the scene depth. Consequently, if we are able to construct $t(x)$, the depth information can recover without any extra information.

B. Dark Channel on Transmission and Atmospheric Light

Dark channel prior is an algorithm used to estimate the transmission map and atmospheric light from outdoor hazy image. Except of sky patches, the principle of DCP is that at least one color channel has very low intensity, which may be close to zero. For this reason, it can estimate a distribution of haze from outdoor image. The smallest channel J^{dark} intensity is expressed in Eq. (3).

$$J^{dark}(x) = \min_{y \in \Omega(x)} \left(\min_{c \in \{r,g,b\}} J^c(y) \right) \quad \textbf{(3)}$$

where J^c is the input image, $\Omega(x)$ is a patch centered at pixel *x*, $\min_{c\in\{r,g,b\}}$ is a min channel, and $\min_{y\in\Omega(x)}$ is a min filter. As mentioned above, DCP is able to accurately estimate the distribution of haze and compute the initial transmission map as Eq. (4).

$$t_D(x) = 1 - \omega \min_{y\in\Omega(x)}\left(\min_{c\in\{r,g,b\}}\frac{I^c(y)}{A^c}\right) \quad \textbf{(4)}$$

where ω is a coefficient utilized to make the recovered image naturally and set to be 0.95. A^c is the brightest pixel value selected from the top 0.1% pixels in the dark channel image. After that, the transmission map and atmospheric light are estimated to recover the scene radiance by Eq. (5), which is transformed from Eq. (1).

$$J^c(x) = \frac{I^c(x) - A^c}{t(x)} + A^c \quad \textbf{(5)}$$

C. Channel-weighted Tuning

The channel-weighted tuning is used to redistribute the color of image. This method can reduce unnatural details of outcome. First, the averages of color channels are computed from hazy image individually by Eq. (6).

$$avg_c = \frac{\sum_{i=1}^{M}\sum_{j=1}^{N} I^c(i,j)}{M\times N}, \quad \text{for} \quad c\in\{r,g,b\} \quad \textbf{(6)}$$

where *M* and *N* are width and height of an input image, I^c expresses a color channel of input image, and the revised values Z_r , Z_g , and Z_b are estimated as follows.

$$Z_r = (avg_g + avg_b)/2 \quad \textbf{(7)}$$

$$Z_g = (avg_r + avg_b)/2 \quad \textbf{(8)}$$

$$Z_b = (avg_r + avg_g)/2 \quad \textbf{(9)}$$

Then, Eq. (10) is followed by revised averages Eqs. (7)-(9) to find a suitable weight s^c :

$$s^c = q\times(avg_r + Z_c)/2, \ \text{for}\ c\in\{r,g,b\} \quad \textbf{(10)}$$

where *q* is a weight value and set to be 0.1. Finally, the channel-weighted tuning is calculated by Eq. (11), which is combined by Eq. (5) and Eq. (10). The haze-free image $J^c(x)$ is derived as follows:

$$J^c(x) = \frac{I^c(x) - (A^c - s^c)}{\max(t_e(x), t_0)} + \left(A^c - s^c\right), \quad \text{for}\ c\in\{r,g,b\} \quad \textbf{(11)}$$

where I^c is the intensity of hazy image, $t_e(x)$ is a transmission map generating from the depth estimation, t_0 is a limitation of transmission map that is set to be 0.1, and A^c is the atmospheric light.

D. The Concept of Brightness Map

The brightness map is an opposite concept to the DCP. As we known, if the objects are similar to atmospheric light and no shadow exists on the scene, it may cause DCP failure and lead to a dim result. To prevent this situation, the brightness map is adopted to compensate the weakness of DCP. Also, it can reflect the illumination of local region from image. Brightness map I^{bright} is expressed in Eq. (12).

$$I^{bright}(x) = \max_{y\in\Omega(x)}\left(\max_{c\in\{r,g,b\}} I^c(y)\right) \quad \textbf{(12)}$$

where $\max_{c\in\{r,g,b\}}$ is max channel, $\max_{y\in\Omega(x)}$ is max filter, and I^c is intensity of image.

In order to enhance the contrast of brightness map, the linear stretching is applied in Eq. (13).

$$t_B(x) = \frac{I^{bright}(x) - \min(I^{bright}(x))}{\max(I^{bright}(x)) - \min(I^{bright}(x))} \quad \textbf{(13)}$$

where $\max(I^{bright}(x))$ is a maximum value in hazy image, and $\min(I^{bright}(x))$ is a minimum value in hazy image. Taking the Figure 2(a) for illustration, the differences of dark channel and brightness map are shown as Figure 2(b) and Figure 2(c). It is obvious that brightness map can fully reflect the bright information.

(a) (b) (c)

Figure 2. Diagram of dark channel and brightness map (a) "White house" with hazy (b) Dark channel of "White house" with Ω = 15×15 (c) Brightness map of "White house" with Ω = 15×15

3 The Proposed Mechanism

The framework is shown in Figure 3, which consists of four phases, illumination determination, sky weight detection, fusion transmission strategy, and luminance enhancement.

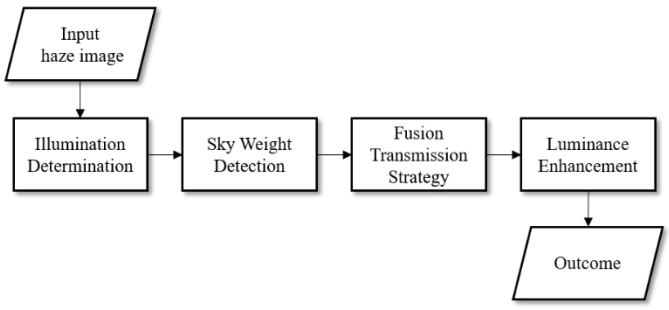

Figure 3. The framework of proposed mechanism

Phase 1. Illumination Determination

We use the characteristics of DCP and brightness map to determine the image as dark or bright. According the result of determination, we employ the adaptive local thresholds (Niblack) [23] on histogram. The details are described as follows.

Step 1. Estimate the corresponding transmission map t_D and t_B of input by Eq. (4) and Eq. (13), respectively.

Step 2. Calculate the Niblack thresholds TH_d and TH_b from t_D and t_B. The block size is set to be $s \times s$.

Step 3. Generate a F_{map} according to Eq. (14):

$$F_{map} = \begin{cases} \text{Bright, If } t_B \geq TH_b \text{ and } t_D < TH_d, \\ \text{Dark, If } t_D \geq TH_d, \\ \text{Otherwise.} \end{cases} \quad \textbf{(14)}$$

Step 4. Obtain the atmospheric light A_{final} according to Eq. (15):

$$A_{final} = \begin{cases} A_{mix}, \text{ If } F_{bpixel} > F_{dpixel} \\ A^c \text{ , Else.} \end{cases} \quad \textbf{(15)}$$

where F_{bpixel} and F_{dpixel} are the sum of bright pixels and dark ones in F_{map}, respectively. If the majority of F_{map} is a bright pixel, we denote the input to be the bright image (*BI*). Otherwise, it is considered as the dark image (*DI*). After that, we apply the *BI* to estimate the revised atmospheric light A_{mix}, which is described in Eq. (16).

$$A_{mix} = (A^c + A_{avg}) / 2 \quad \textbf{(16)}$$

where A_{avg} is the average of hazy image.

After completing the first phase, an outcome of *BI* is led to the phase 3 to calculate the transmission; otherwise, an output of *DI* is guided to the phase 2 for further detection.

Phase 2. Sky Weight Detection

The sky weight detection is to judge whether the input has the sky area or not and separate the hazy image into foreground and background according to the illumination, gradient, and gray level pixel. Afterwards, the weight maps are computed from *DI*, and three sky features are set to different weight values individually. Also, we combine three weight maps into the weighting map, as shown in Figure 4(b) and Figure 4(e). After that, the detected results are displayed in Figure 4(c) and Figure 4(f). According to the results, we can distinguish the sky image (*SI*) from non-sky image (*NSI*) in Figure 4(a) and Figure 4(d), respectively. The details of process are shown as follows.

Step 1. Calculate both DCP and brightness map from input image. Two thresholds α and β are set to create a weight map *b* based on Eq. (17).

$$b = \begin{cases} 1, \text{ If } DC \geq \alpha \,\&\, BM \geq \beta, \\ 0, \text{ Otherwise.} \end{cases} \quad \textbf{(17)}$$

where *DC* is dark channel, *BM* is brightness map, and *b* is weight map of illumination.

Step 2. Estimate the gradient *G* of input image, and set the threshold γ to construct a weight map *e* by Eq. (18).

$$e = \begin{cases} 1, \text{ If } G \leq \gamma, \\ 0, \text{ Otherwise.} \end{cases} \quad \textbf{(18)}$$

Step 3. Build the gray level image *GI*, and set the threshold δ to create a weight map *g* according to Eq. (19).

$$g = \begin{cases} 1, \text{ If } GI \geq \delta, \\ 0, \text{ Otherwise.} \end{cases} \quad \textbf{(19)}$$

Step 4. Construct weighting map *W* via Eq. (20). The results are shown in Figure 5(b) and Figure 5(e):

$$W = p * b + q * e + t * g \quad \textbf{(20)}$$

where *p*, *q*, and *t* are weight values of illumination, gradient, and gray level pixel.

Step 5. Select the major region by threshold ω on weighting map *W* and divide the image into the foreground and background according to Eq. (21). r = 1 indicates that the region is marked as sky part, and r = 0 means the area of foreground.

$$r = \begin{cases} 1, \text{ If } W \geq \omega, \\ 0, \text{ Otherwise.} \end{cases} \quad \textbf{(21)}$$

Step 6. Count the proportion of the sky region that is labeled from the whole image. If the proportion is smaller than 5%, as displayed in Figure 4(f), we denote the input image as *NSI*; otherwise, we set the input image as *SI*. After that, the detected result of *SI* is segmented into two parts of scene via Eq. (21), as demonstrated in Figure 4(c). Note that the *NSI* will not refer to the detected result *r*.

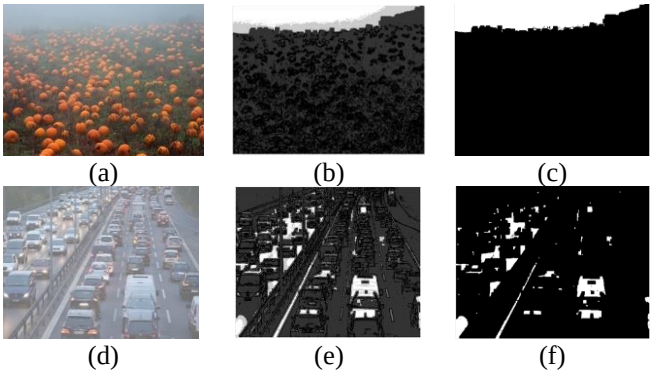

(a) (b) (c)

(d) (e) (f)

Figure 4. The results of sky weight detection
(a) Input image "Pumpkin" (b) Weighting map from "Pumpkin" (c) Detected results from "Pumpkin" (d) Input image "Traffic"

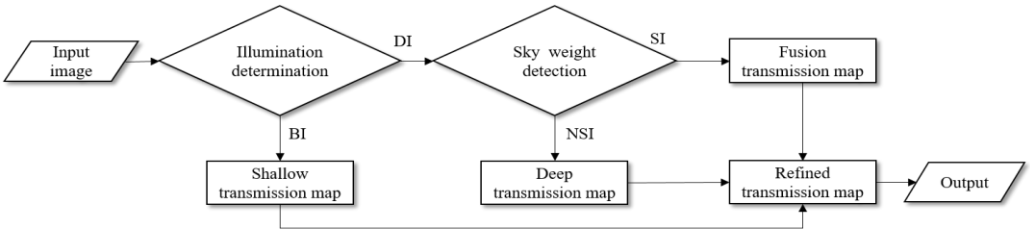

Figure 5. The flowchart of fusion transmission strategy

(a) (b) (c) (d) (e)

Figure 6. Procedure of fusion transmission map
(a) Input image (b) Shallow transmission map (c) Deep transmission map (d) Fusion transmission map (e) Refined transmission map

Phase 3. Fusion Transmission Strategy

The strategy is used to adaptively create the different transmissions on image according to the results of illumination determination and sky weight detection. The labels of image include *BI*, *SI*, and *NSI*. The flowchart is shown in Figure 5. We focus on the individual calculation of transmission under different conditions. Taking Figure 6(a) for example, when the input is *BI* then we compute the shallow transmission. The result is shown in Figure 6(b). If the input is *DI* and marked as a *NSI*, we calculate the deep transmission, as displayed in Figure 6(c). While the image is determined as *DI* and *SI*, we construct the fusion transmission combined with Figure 6(a) and Figure 6(b), as demonstrated in Figure 6(d). Finally, we apply the guided filter [22] to avoid the block effect on transmission map in Figure 6(e). The details of procedure are illustrated as follows.

Step 1. Estimate the transmission t_k according to Eq. (22).

$$t_k = \begin{cases} t_{sh,} \text{ If } I^c = BI, \\ t_{de,} \text{ Else if } I^c = NSI, \\ t_{f,} \text{ Else if } I^c = SI. \end{cases} \tag{22}$$

where I^c is the input image, and *BI*, *SI*, and *NSI* are the judgment results from the phase 1 and phase 2, and t_{sh} is the shallow transmission in Eq. (23), which is modified according to [16].

$$t_{sh}(x) = 1 - \omega \min_{y \in \Omega(x)} \left(\min_{c \in \{r,g,b\}} I^c(y) \right) \tag{23}$$

t_{de} is the deep transmission which is in line with the boundary constraint [10] according to Eq. (24) and Eq. (25).

$$t_s(x) = \underset{x \in \omega_x}{\text{closing}}\ t_b(x) \tag{24}$$

$$t_b(x) = \min(1, \max_{c \in \{r,g,b\}} (\frac{I^c(x) - A^c}{C^c_{low} - A^c}, \frac{I^c(x) - A^c}{C^c_{high} - A^c})) \tag{25}$$

where closing(.) is a closing operator of morphological image processing, C_{low} and C_{high} are low and high constraints, respectively. A^c is the brightest pixel. In order to avoid high contrast of recovered image, we improve the deep transmission t_{de} via Eq. (26), which is the average value of the strong transmission t_s and shallow transmission t_{sh}.

$$t_{de} = (t_s + t_{sh}) / 2 \tag{26}$$

t_f is the fusion transmission in Eq. (27), which is integrated by t_{sh} and t_{de}.

$$t_f = t_{sh} \cap t_{de} \tag{27}$$

According to the detected result *r* from Eq. (21), we can figure out the foreground and background of an image. Next, t_{sh} and t_{de} are adopted in the parts of background and foreground, respectively.

Step 2. Refine the transmission map based on Eq. (28):

$$t_r(x) = G(t_k(x)) \tag{28}$$

where *G* is guided filter [22].

Phase 4. Luminance Enhancement

We recover the image according to Eq. (29), which is calculated via Eq. (15) and Eq. (28). Afterwards, we enhance the luminance of recovered image for getting the image clearly.

$$\hat{J}^c(x) = \frac{I^c(x) - (A_{final}{}^c - s^c)}{\max(t_r(x), t_0)} + \left(A_{final}{}^c - s^c\right), \text{ for } c \in \{r,g,b\} \tag{29}$$

Step 1. Convert the RGB color space of $\hat{J}^c$, named $\hat{J}_{RGB}$, into Lab color space through Eq. (30).

$$\hat{J}_{RGB} \rightarrow J_{LAB} \tag{30}$$

Step 2. Stretch the luminance L of J_{LAB} to the range between [0, 255] according to Eq. (31).

$$J_{LAB} \rightarrow J_{L'AB} \tag{31}$$

Step 3. Translate the modified Lab color space to RGB color space based on Eq. (32).

$$J_{L'AB} \rightarrow J_{RGB'} \tag{32}$$

Step 4. Revise the weight values v and u according to Eq. (33). Then, we output the result.

$$\tilde{J} = v * \hat{J}_{RGB} + u * J_{RGB'} \tag{33}$$

4 Experimental Results and Analysis

The experimental environment is described as follows. A personal computer installed with Windows 10 64-bit is applied to simulate the system, equipped with an Intel Core I7-4770HQ 3.4-GHz with 8G RAM. The software used to modify the image is Adobe Photoshop CS6, and all algorithms were implemented in the MatlabR2017b environment. Aside from a subjective assessment from human vision to measure the performance of our proposed method, we have adopted two objective indexes to examine the quality of refined image.

The test images contain natural targets and artificial ones. Both of them could be further separated into two categories, sky picture and non-sky photo. The used nature images are selected from classical dehazing researches [7-10]. The source of artificial image is an open database named Flicker and INRIA Holidays datasets [25]. INRIA Holidays dataset [25] contains 1941 images including landscape and architecture. To prove the capability of dehazing a bright photo, which is a crucial challenge in the field of removing haze, we also selected images containing white objects as the test targets.

Parameters in the simulations are defined in the following. The block size of Niblack is set to 15×15, while the gray level δ is tuned to be 0.7 referred to [20]. As to the threshold of sky weight detection, the dark channel α and brightness map β are adjusted to 0.6, and the gradient threshold γ is defined as 0.2. Due to the fact that the illumination is an important factor in the sky, we have the setting of p = 0.6, q = 0.2, and t = 0.2, while the threshold of weight map ω is set to 0.4. Regards to the parameters of luminance enhancement phase, v and u stay at 0.5. The reason is that the setting of u =1 might lead to an unnatural result. Thus, the average of these two parameters could bring in a proper distribution of luminance.

We have simulated the parameter combination to find out a preference matching through exhaustive method, where the number of all combinations is 39,600,000 between (0, 1], the unit is 0.1. The restriction includes that the sum of p, q, and t is 1 from Eq. (20), the sum of v and u is 1 from Eq. (33). Also, the dehazing effect will be decreased if ω is lower than 0.3 due to disregarding the sky area in Phase 2 of section 3. If the parameters v and u are lower than 0.3 or are higher than 0.7, the dehazed image will result in underexposed or overexposed. Therefore, the total simulation combination is 756,000 after we exclude the above conditions. The thresholds used in the proposed scheme are marked as red in Table 1. Both PSNR and SSIM values of the used combination are better than others. We retain good human visual outcomes in the corresponding dehazed images, as shown in Figure 7 to Figure 13. Contrarily, if we over adjust the thresholds, it will lower down the image quality of detail and the lightness.

Table 1. The output of different threshold combinations

α	β	γ	δ	p	q	t	v	u	w	PSNR(dB)	SSIM
0.1	0.1	0.1	0.1	0.1	0.1	0.8	0.4	0.6	0.4	23.78	0.9240
0.1	0.1	0.1	0.1	0.1	0.1	0.8	0.4	0.6	0.5	23.78	0.9240
0.1	0.1	0.1	0.1	0.1	0.1	0.8	0.4	0.6	0.6	23.78	0.9240
⋮	⋮	⋮	⋮	⋮	⋮	⋮	⋮	⋮	⋮	⋮	⋮
0.2	0.2	0.4	0.3	0.2	0.2	0.6	0.6	0.4	0.5	23.66	0.9204
0.2	0.2	0.4	0.3	0.2	0.2	0.6	0.6	0.4	0.6	23.43	0.9135
0.2	0.2	0.4	0.3	0.2	0.2	0.6	0.6	0.4	0.7	23.43	0.9135
0.2	0.2	0.4	0.3	0.2	0.2	0.6	0.6	0.4	0.8	23.43	0.9135
0.2	0.2	0.4	0.3	0.2	0.2	0.6	0.6	0.4	0.9	22.92	0.9095
0.2	0.2	0.4	0.3	0.2	0.2	0.6	0.6	0.4	1	22.92	0.9095
⋮	⋮	⋮	⋮	⋮	⋮	⋮	⋮	⋮	⋮	⋮	⋮
0.6	0.6	0.2	0.7	0.6	0.2	0.2	0.4	0.6	0.9	23.78	0.9168
0.6	0.6	0.2	0.7	0.6	0.2	0.2	0.4	0.6	1	23.78	0.9153
0.6	**0.6**	**0.2**	**0.7**	**0.6**	**0.2**	**0.2**	**0.5**	**0.5**	**0.4**	**24.15**	**0.9376**
0.6	0.6	0.2	0.7	0.6	0.2	0.2	0.5	0.5	0.5	23.69	0.9224
0.6	0.6	0.2	0.7	0.6	0.2	0.2	0.5	0.5	0.6	23.69	0.9224
⋮	⋮	⋮	⋮	⋮	⋮	⋮	⋮	⋮	⋮	⋮	⋮
1	1	1	1	0.8	0.1	0.1	0.6	0.4	0.8	22.71	0.9095
1	1	1	1	0.8	0.1	0.1	0.6	0.4	0.9	22.74	0.9095
1	1	1	1	0.8	0.1	0.1	0.6	0.4	1	22.74	0.9063
									Average	23.50	0.9189

To emphasize the contributions, we compared the dehazing methods including He et al. [9], Meng et al. [10], Huang et al. [11], Berman et al. [12], Zhu et al. [15], Lee et al. [16], Peng et al. [17], and Shin et al. [25] with the new one in terms of subjective and objective indexes. Researches in [9-11] are classical dehazing algorithms, while those of [12, 15-17, 25] are the latest works. Specially, Peng et al. [17] could achieve generalization under multiple environmental conditions consisting of fog, sandstorm, underwater and night image. Here, we only focus on foggy images as the goal of most related works is applied to enhance the quality of such targets. The examination of natural image is illustrated in Section A, and the performance of artificial image is demonstrated in Section B.

A. Experimental results of natural image

First, we analyze the dehazed results on human visual perception, and the natural image is captured by camera. In order to verify the effectiveness of our method, the test images we used include "air particle", "pumpkin", "straw", "red brick", and "city" which are common adopted in dehazing researches. Figure 7(a) displays the original "air particle", which is a natural picture containing strong air pollution. The refined results from related works [9-12, 15-17, 25] are listed in Figure 7(b) to Figure 7(i). No doubt that these methods can remove most fogs in the test image successfully. The red circle, however, is used to highlight the refinement difference between related works and ours. It is apparent that circles in the results of [9, 10, 12, 15, 25] have drawn serious color distortion at the sky region, as illustrated in Figure 7(b), Figure 7(c), Figure 7(e), Figure 7(f), and Figure 7(i), which is an unnatural consequence in the real world. The main reason is that the transmission map is adopted with the same intensity. Thus, it may cause the overexposure to the sky region. Considering the fact that there exists only few structure in the background of an image, it is unnecessary to count atmospheric light in removing the haze. The results of [11, 16] are shown in Figure 7(d) and Figure 7(g). As the channel analysis is utilized to avoid the overexposure, which is good at balancing the color of image, the haze located at the sky region could be cleared successfully. Nevertheless, taking insight into the red circle, it is not difficult to learn that the fog stays on the building cannot be removed well in comparison with the new results, as depicted in Figure 7(j). It is due to the adoption of deep transmission in our mechanism, which can be used to help layout a scene preserving natural contrast. Moreover, the visual effect of Peng et al. [17] is as good as ours, as illustrated in Figure 7(h) illustrates the outcome. The main reason is that [17] adopted the linear regression, which is capable of dehazing an image under various weather conditions.

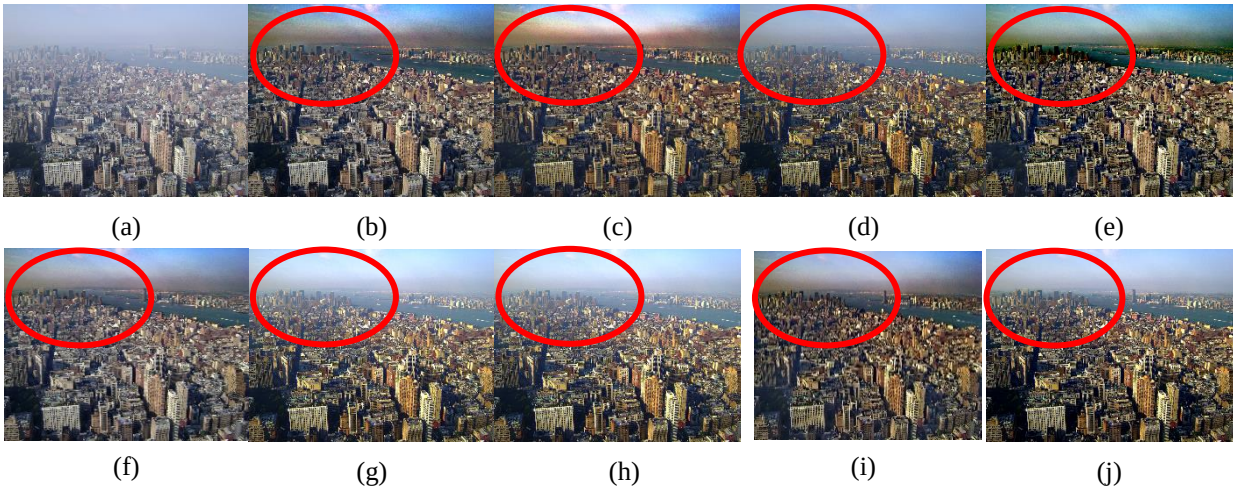

Figure 7. Comparisons of with a natural image of air particle
(a) Input image (b) He et al. [9] result (c) Meng et al. [10] result (d) Huang et al. [11] result (e) Berman et al. [12] result (f) Zhu et al. [15] result (g) Lee et al. [16] result (h) Peng et al. [17] result (i) Shin et al. [25] result (j) The proposed method

The photo "pumpkin" has the similar color and duplicate objects, as displayed in Figure 8(a). The results of related methods are exhibited in Figure 8(b) to Figure 8(i). In order to highlight the consequent, the green block is used to denote the foreground, while the red one is employed to represent the background. Regarding to the red block, when the methods of [11, 15-16] are implemented in Figure 8(a), they could reduce the color shifting effectively. The main reason is that [11, 16] have adopted the channel analysis, the background could be layout in a better result, as illustrated in Figure 8(d) and Figure 8(f). Also, due to the fact that [15] has estimated the transmission by minimizing the energy function, it can maintain the illumination of image, as shown in Figure 8(g). As to the green block of [11, 15-16, 25], it is obvious that the structure is unclear and the contrast is decreased in comparison with the outcome of our method. Regards to the result shown in Figure 8(j), it has demonstrated the performance of the new method, which is able to produce a satisfactory quality on foreground and background, respectively. The key point is that the fusion transmission strategy is applied in our technique. More precisely, the shallow transmission is used to deal with the background, and the deep transmission is applied to the foreground.

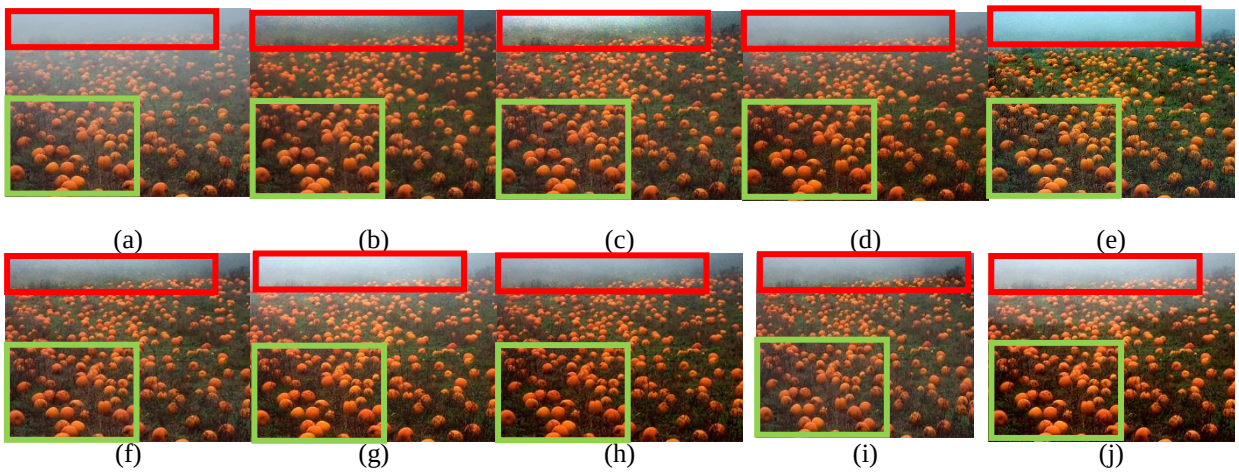

Figure 8. Comparisons of with a natural image of pumpkin
(a) Input image (b) He et al. [9] result (c) Meng et al. [10] result (d) Huang et al. [11] result (e) Berman et al. [12] result (f) Zhu et al. [15] result (g) Lee et al. [16] result (h) Peng et al. [17] result (i) Shin et al. [25] result (j) The proposed method

The third challenge is to recover a foggy image "straw" shown in Figure 9(a). Both the background and foreground possess a similar color and scene, and parts of the background structure need to be recovered. The difficulty of telling the background from the foreground often dominates the recovery performance of entire image. Outcomes of related methods and the new method are exhibited in Figure 9(b) to Figure 9(i). The red blocks are used to emphasize the dehazed results of the background. It is clear that [11, 16], and [25] cannot remove the haze well but avoid the overexposure on the background, as displayed in Figure 9(d), Figure 9(g), and Figure 9(i). It is owing to that the adoption of weak transmission may lead to the failure of recover the image structure. In regard to the results of [10, 12, 17], as shown in Figure 9(c), Figure 9(e) and Figure 9(h), the hazed areas of background have been removed clearly. Nevertheless, there exists serious color distortion at the sky region. The main reason is that the strong transmission is applied to whole image. Thus, it can dehaze the image clearly but layout the color distortion at the white area. Inspired by above observation, we have learned that the weak and strong transmissions are not always suitable for renovating all the hazed areas. In the proposed method, we have introduced the fusion strategy to find a favorable solution, in which the shallow transmission map is used to deal with a bright scene, while the deep one is applied to refine a non-sky region. Therefore, the new method can recover specific regions suitably, including providing a clear image structure and escaping from an overexposure background, as displayed in Figure 9(j).

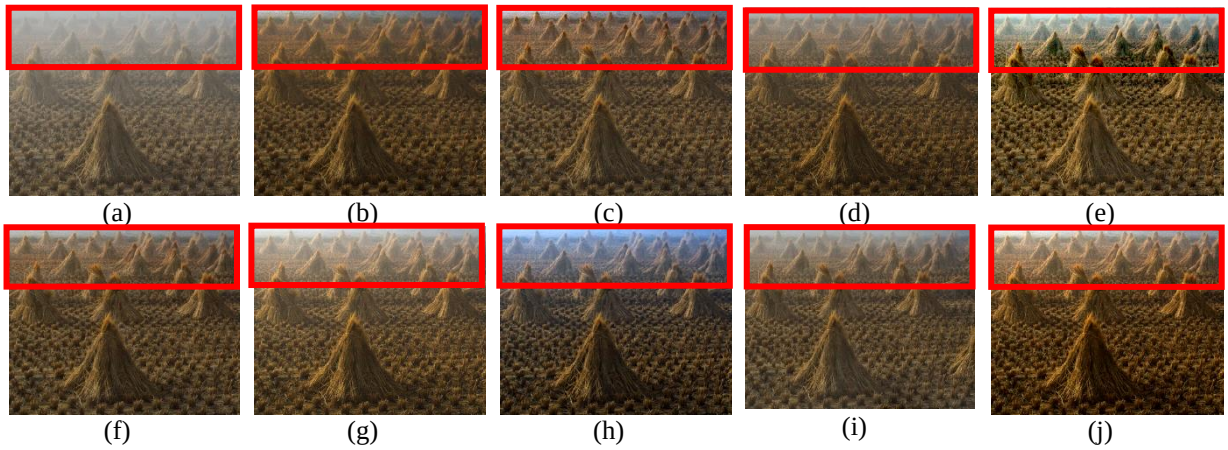

Figure 9. Comparisons of with a natural image of straw
(a) Input image (b) He et al. [9] result (c) Meng et al. [10] result (d) Huang et al. [11] result (e) Berman et al. [12] result (f) Zhu et al. [15] result (g) Lee et al. [16] result (h) Peng et al. [17] result (i) Shin et al. [25] result (j) The proposed method

Figure 10(a) illustrates a "red brick", which is a haze image without the sky. The dehazed results of related works are exhibited in Figure 10(b) to Figure 10(i). In Figure 10(b) to Figure 10(g) and Figure 10(i), the fog can be removed successfully, but the illumination of the dehazed image is unnatural, either too bright or dark. Concerning to the result of Peng et al. [17], it has serious color shifting, as displayed in Figure 10(h). This is due to that the main color predicted by linear regression is red, which may mislead to deal with a sandstorm image. According to the stage of sky weight detection in the new method, Figure 10(a) is regarded as a non-sky image. Thus, the deep transmission map is employed to

eliminate the fog. Hereafter, the RGB channels of provisional outcome is tuned to Lab color space. Next, the histogram stretching is applied to "L" to produce the final result. As shown in Figure 10(j), the new method can not only remove the fog effectively but also keep the "red brick" with a natural and saturated color.

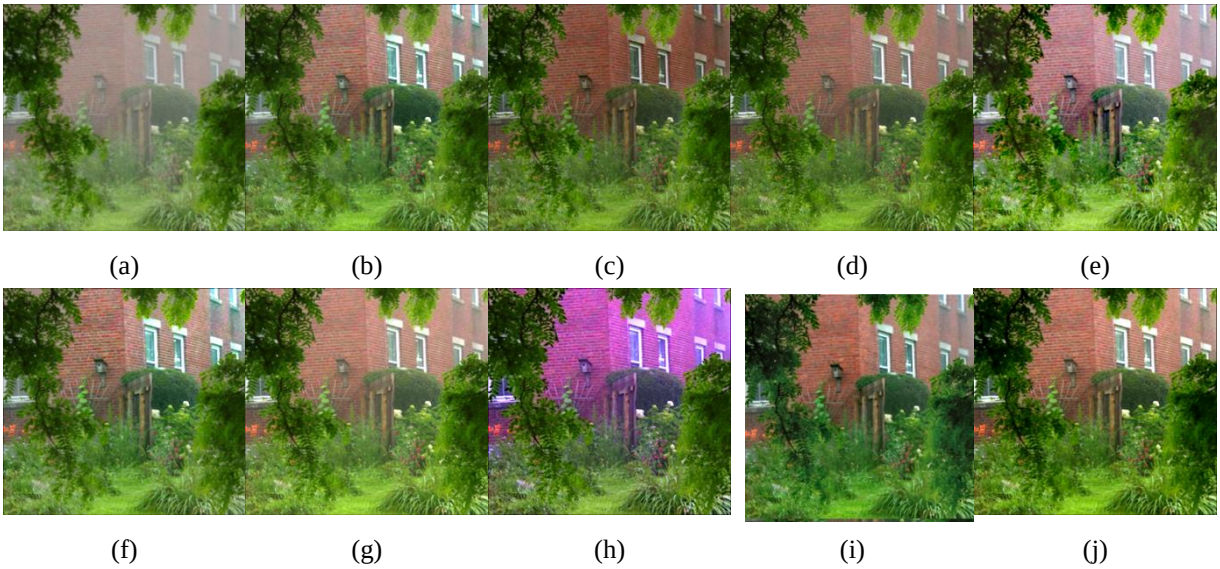

(a) (b) (c) (d) (e)

(f) (g) (h) (i) (j)

Figure 10. Comparisons of with a natural image of red brick
(a) Input image (b) He et al. [9] result (c) Meng et al. [10] result (d) Huang et al. [11] result (e) Berman et al. [12] result (f) Zhu et al. [15] result (g) Lee et al. [16] result (h) Peng et al. [17] result (i) Shin et al. [25] result (j) The proposed method

In the following, we examine the dehazing capability in dealing with the test image "city" containing sky region and white object simultaneously, as shown in Figure 11(a). The refined outcomes of [9-12, 15] are displayed in Figure 11(b), to Figure 11(f). The restored color of foreground is like the original scene, but the background cannot be well recovered through these methods. More precisely, they cannot bring a vivid hue for the region of sky due to the adoption of strong transmission map. In contrast to above consequences, Figure 11(g) to Figure 11(i) have revealed better results of [16-17] and the new method because of the employment of weak recovery. To highlight the superiority of the new method, we marked the white building with a red rectangle and enlarged it in Figure 12. As displayed in Figure 12(a), there exist black lines to disturb the straight structure of the building. On the other hand, Figure 12(b) has brought an obscure structure of the whole building. Concerning to the outcome of Figure 12(c), the structure and color of main target are well refined. It is due to the help of illumination determination and adaptive estimation of atmospheric light.

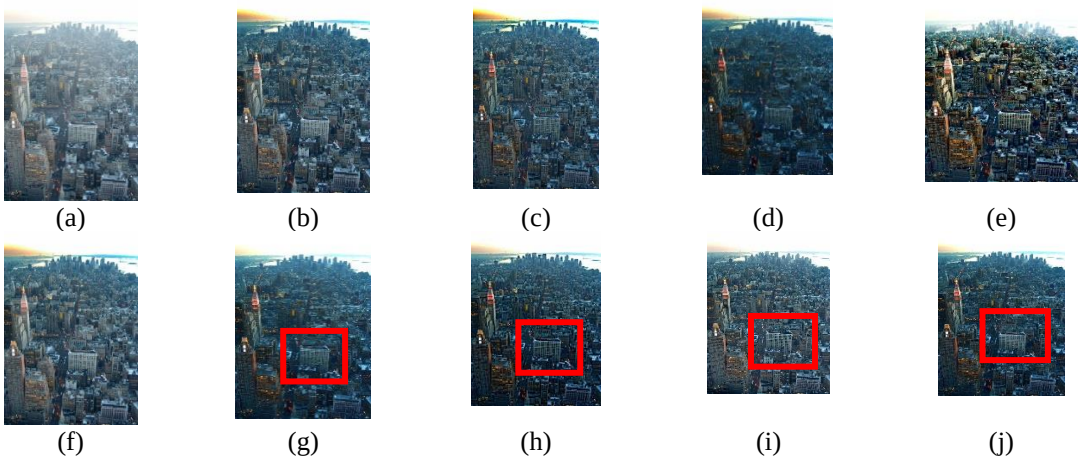

(a) (b) (c) (d) (e)

(f) (g) (h) (i) (j)

Figure 11. Comparisons of with a natural image of city
(a) Input image (b) He et al. [9] result (c) Meng et al. [10] result (d) Huang et al. [11] result (e) Berman et al. [12] result (f) Zhu et al. [15] result (g) Lee et al. [16] result (h) Peng et al. [17] result (i) Shin et al. [25] result (j) The proposed method

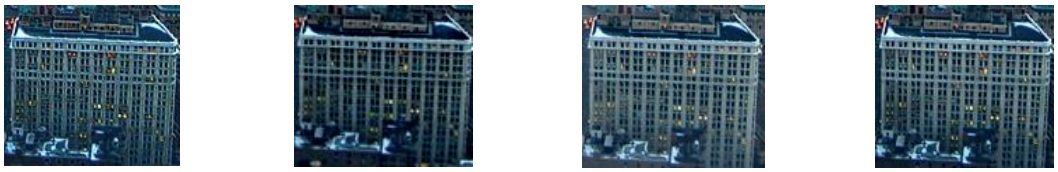

(a) (b) (c) (d)

Figure 12. Comparisons of with a natural image of city for white building
(a) Lee et al. [16] result. (b) Peng et al. [17] result. (c) Shin et al. [25] result (d) The proposed method.

As demonstrated in Figure 7 to Figure 12, the proposed method can deal with the details effectively and avoid the overexposure from the sky. The key factor is the fusion strategy of transmission. In fact, the background is often formed by the sky area and strong fog, in which the excessive recovery is unnecessary as the proportion of haze is low. Based on this observation, we have learned that a shallow transmission is more appropriate to the background and bright scene, while a deep transmission is suitable for recovering the color and structure of the foreground.

B. Experimental results of artificial image

To demonstrate the contribution from an objective point of view, we have examined the capability of these methods via artificial images. Since it is difficult to capture a pair of hazy and hazy-free images displaying the same scene through a camera, we need to synthesize a hazy image from haze-free image, while the haze-free image is chosen from the Flickr and INRIA Holidays dataset [24] and regarded as the ground truth (GT). Here, we have adopted two quantitative criteria to evaluate the performance, including PSNR and SSIM values. These two indexes are the significant ones used to define the image quality by computing the similarity between a noise-free image and a dehazed one. The test data includes the GT and dehazed image. The higher index value displays that it possesses better capability of recovering a hazy image. The unit of PSNR is shown as decibels (dB). The main concept is to compare the Mean Squared Error (MSE) of two images. If the MSE value is small, it represents the difference between images are tiny. The formula as follows:

$$PSNR = 10 \times log_{10}(\frac{255^2}{MSE}) \quad \textbf{(34)}$$

$$MSE = \frac{\sum_{i=1}^{M}\sum_{j=1}^{N}(GT_{i,j}-J_{i,j})^2}{M \times N} \quad \textbf{(35)}$$

where $M \times N$ is the size of image, $GT_{i,j}$ is the GT, and $J_{i,j}$ is the recovered image. On the other hand, the SSIM is applied to compare three factors of two images, including luminance, contrast, and structure information. It is due to the fact that these features are more sensitive to the human vision system. The value of SSIM ranges from 0 to 1. When the assessment value is close to 1, it means that the dehazed image is approximated to the hazy-free one.

$$SSIM = \frac{(2\mu_x\mu_y+C_1)(2\sigma_{xy}+C_2)}{(\mu_x^2+\mu_y^2+C_1)(\sigma_x^2+\sigma_y^2+C_2)} \quad \textbf{(36)}$$

where μ_x is the average of recovered image $J=\{J_{i,j}\}$, μ_y is the average of ground truth $GT=\{GT_{i,j}\}$, σ_x^2 and σ_Y^2 are the covariance of recovered image and ground truth, respectively. C_1 and C_2 are the constants defined as $C_1=(K_1L)^2$ and $C_2=(K_2L)^2$, where K_1=0.01, K_2=0.03 are defined by default, and L = 255 is the dynamic range of a pixel.

Figure 13 displays four images from public database, including R1: "Building", R2: "Landscape", R3: "Houses", and R4: "Highway". First, we analyze the sky regions of these results according to the human vision perception. It is apparent that other methods have suffered from color shifting and overexposure problem since those methods removed the haze by the unanimous intensity. In contrast, our fusion strategy has utilized the different strength of transmission on the foreground and background; thus, leading to higher PSNR values in all test images. The components of R1 contain bright buildings and a sky region. Taking a deep insight into the background, the results of [12] and ours look more naturally in comparison with those of others. More precisely, serious color shifting happens to the outcomes of related works so that most of structures look too dim to be recognized, compared to the GT. The reason is that the scene is bright, but these techniques only calculate the maximum pixel value as the air light. This might make an improper recovery to darken the scene. By contrast, we have applied the illumination determination to tune the computation of atmospheric light and transmission adaptively. Thus, the new method gains an average PSNR value, which is 10.08 dB higher than those of other works.

R2 represents the "Landscape", which contains clouds in the sky. It is clear that Lee et al. [16] and our method are capable of avoiding the overexposure problem, while it happens to the sky regions of other recovered outcomes. Furthermore, our result can achieve a higher contrast and obvious structure owing to the deep transmission map adoption. In fact, the correctness of separating the background from foreground highly dominates the recovery result. If we only use a single feature such as gray level, it might cause the failure on segmentation. An incorrect segmentation might further mislead the fusion strategy and degrade the quality of image. In order to detect the sky region accurately, the new method observes three features, including illumination, gradient, and gray level, in the sky weight detection. Each of them is set to an individual weight. Hence, the new method can lay out a higher PSNR value in comparison with related works. As to R3, "Houses" contains a large region of architecture, and the scene is quite bright. No doubt that most related methods can remove the fog clearly, but they are unable to obtain a real-like color as all the tuning procedures of recovery are immovable. On the contrary, the proposed method has utilized an adaptive dehazing technique; thus, resulting in an average PSNR value, which is 7.81 dB higher than those of other methods. In R4, it is easy to tell the foreground from background. Thus, most methods can achieve satisfactory dehazed outcomes. However, with a more precise examination, the color shifting has happened to the recovered sky regions of [9-12, 15], while our consequence

can escape from this issue due to the shallow transmission map. It is worth mentioning that the visual effect of [16] is almost equal to that of the proposed method, but its PSNR value is 3.3 dB lower than ours. The main reason is that the adoption of deep transmission can help to lay out a scene with more reality.

From above observation, it is not hard to learn that traditional dehazed techniques cannot deal with white objects well. Taking the outcome of [17] for instance, a well defogged scene has brought the color distortion in comparison with GT. This is due to that this method mainly focus on the generalization of different weathers. In fact, the brighter of atmospheric light, the darker of scene radiance, and vice versa. This has demonstrated the contribution of illumination determination in the new scheme. To highlight the capability of settling the problem of while object and sky region, we further examine the new method in two test images, containing massive white objects. W1: "Merlion" and W2: "White house" are selected from public database. It is obviously that white objects and structures have nearly occupied the entire image, which is a crucial challenge in dehazing. Regarding the case of W1, the observation on the outcomes of related works has demonstrated the absence of brightness, while it is naturally displayed at the sky region in the new method. Even though [15-16], and our method can preserve the PSNR values higher than 20 dB, the foreground structure could not be recovered completely in [16], while the sky region still suffers from color shifting in [15]. That is owing to that other methods have selected the brightest pixel from the top 0.1% pixels of image. Once the input image has apparent white objects, the estimation of atmospheric light must fail. To fix this issue, the brightness map is integrated with dark channel in the new method. Based on these two bases in illumination determination, "Merlion" is considered as a bright image. Hence, the atmospheric light and transmission map could be tuned adaptively.

The second examination on the bright scene is displayed as W2: "White house", in which white objects teem in the image. The result of [15] has shown that the fog could be removed effectively, but the color shifting occurs in the white structure to decay the quality. Concerning to the consequence of [17], multiple weather conditions could be handled well due to the adoption of the linear regression on the color analysis. However, this might lead to the misjudgment of the background and foreground. As the intensity is quite similar, it is not easy to obtain an ideal refined result. W2 has illustrated the superiority of our method to others in terms of subjective human viewing and objective PSNR index.

From Figure 13, it is observed that our method can achieve the better outcomes in comparison with other methods according to the subjective point of view and objective PSNR and SSIM values. To make the objective assessments clearly, the PSNR values of all methods are summarized in a line chart, given in Figure 14. Even the outcomes of [25] are better than those of related works and ours in terms of D2, D3, and D4, the dehazed background of [25] still suffered from color shifting on visual perception. In contrast, the new method has yielded a bright structure and a color shifting-free background. Take a deep look, the outcomes of Shin et al. [25] and ours are definitely better than those of the related words in Figure 14 of D1, D2, D3, and D4, in which D1, D2, D3, and D4 display the fog spread from up to down, down to up, left to right, and right to left, respectively. Moreover, the SSIM values of all methods are depicted in Figure 15. These two charts have shown clearly that the new method outperforms related works in both of the SSIM and PSNR values, which indicating that the new method is able to remove fog and keep that structure simultaneously. Again, it depends on the help of illumination determination and adaptive estimation of atmospheric light according to Eqs. (15) and (22). Aside from that, it makes the structure closer to ground truth via translating the color space to tune the luminance based on Eq. (33).

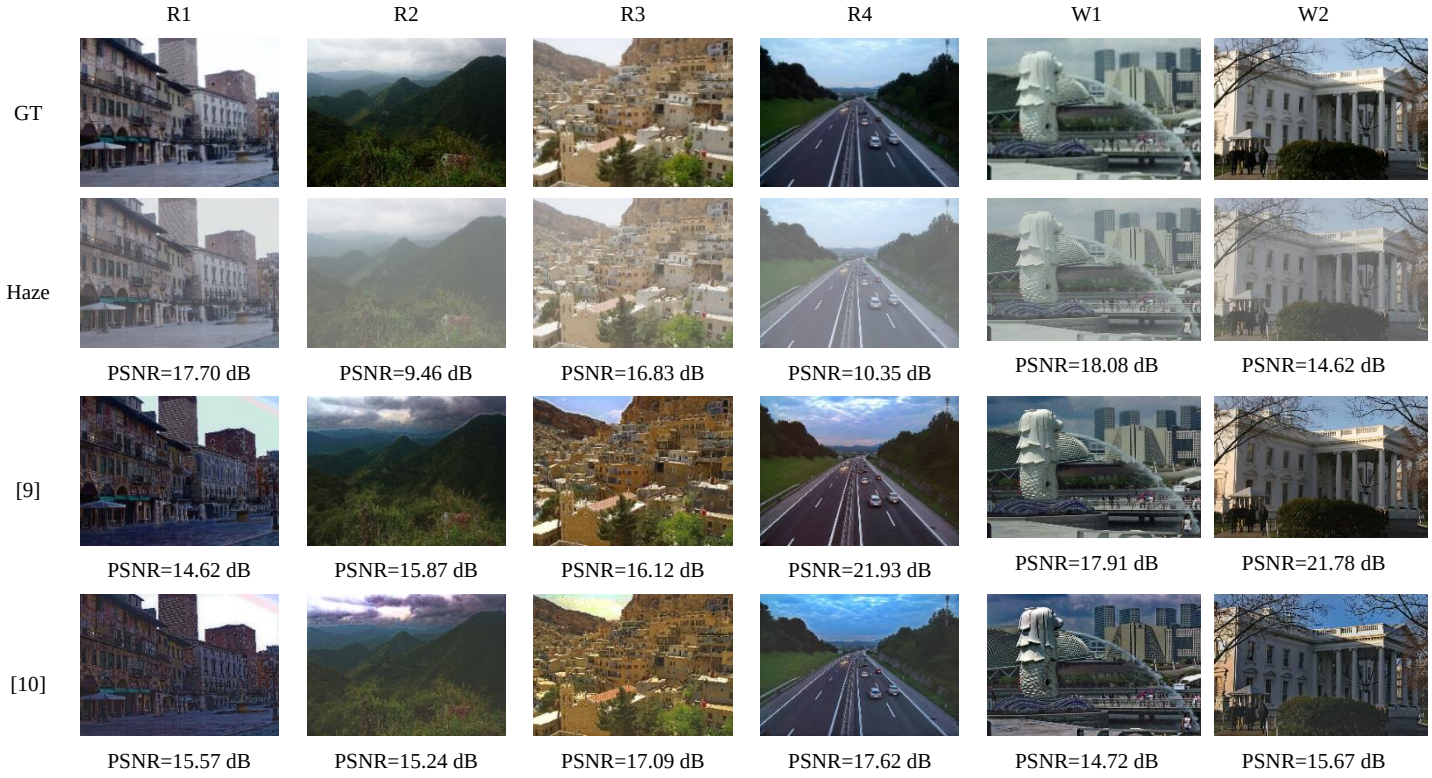

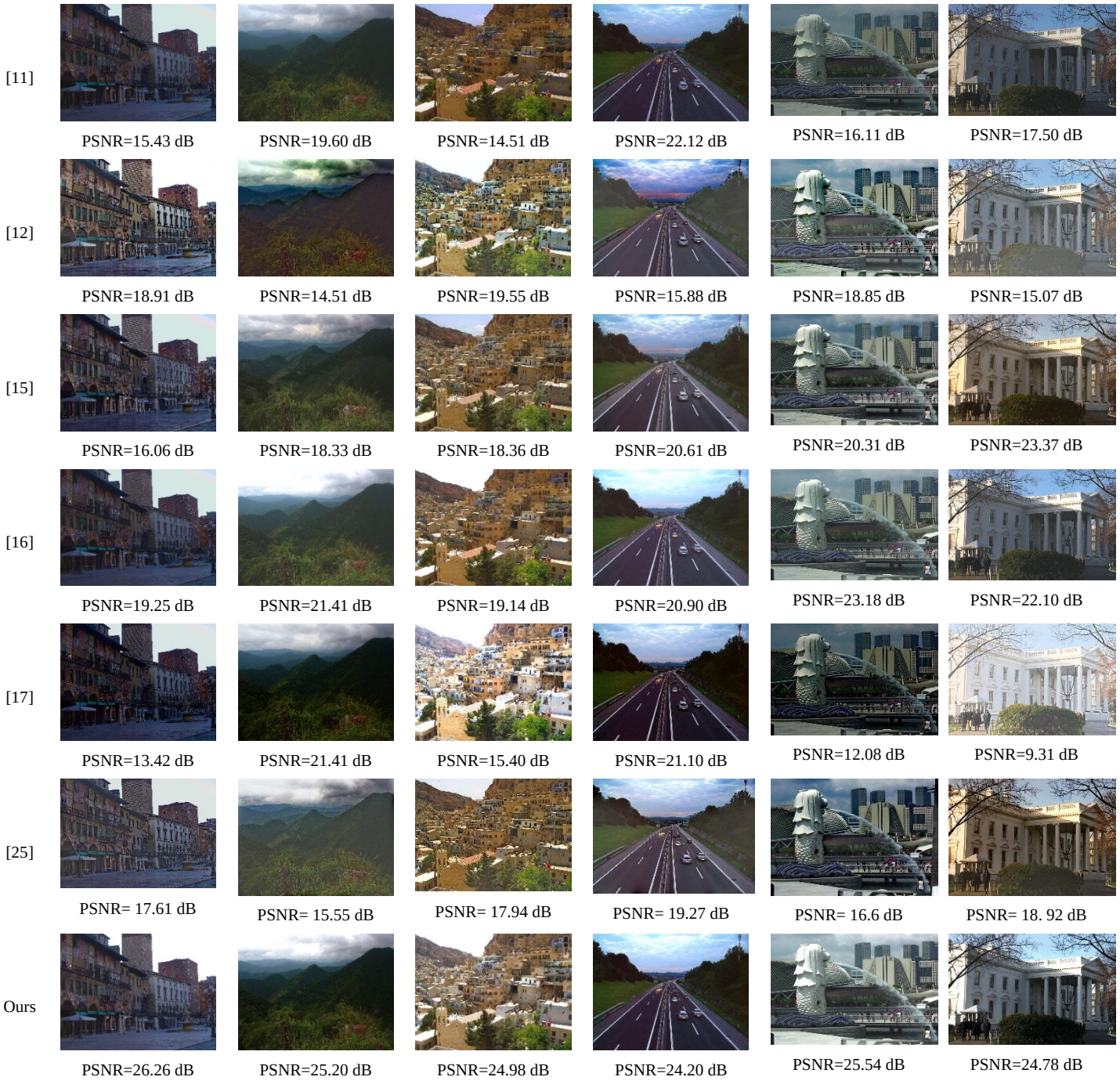

Figure 13. Comparisons of with an artificial image, including R1-R4 and W1-W2

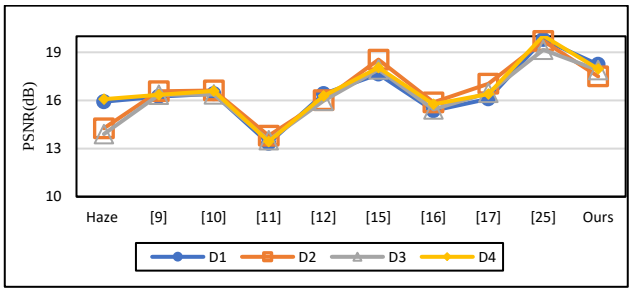

Figure 14. PSNR values from four directions of fog

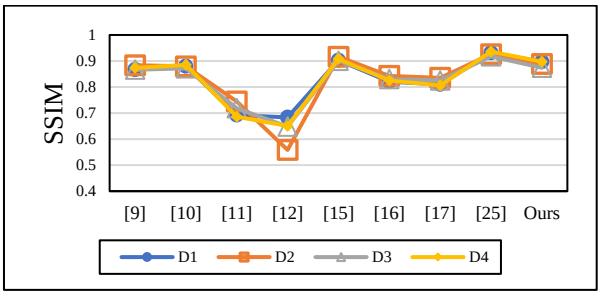

Figure 15. SSIM values from four directions of fog

5 Conclusions

In this article, we have developed an adaptive image dehazing technique based on the fusion transmission and sky weight detection. The illumination determination can be applied to enhance quality of image on the white scene. The fusion transmission can be adopted to recover the specific region via the shallow and deep transmission, which is able to reduce the overexposure and color shifting. Then, the sky weight detection makes the fusion strategy more accurately and generally. Simulation results have demonstrated that the new method can remove the foggy from the haze image effectively from the human vision perception and overcome the problem caused by a large while object. Moreover, the new method can achieve higher PSNR and SSIM values in comparison with related works.

References

[1] J. Kopf, B. Neubert, B. Chen, M. Cohen, D. Cohen-Or, O. Deussen, M. Uyttendaele, D. Lischinski, Deep Photo: Model-based Photograph Enhancement and Viewing, *ACM Transactions on Graphics*, Vol. 27, No. 5, pp. 1-10, December, 2008.

[2] S. G. Narasimhan, S. K. Nayar, Interactive (De) Weathering of an Image using Physical Models, *IEEE Workshop on Color and Photometric Methods in Computer Vision*, Nice, France, 2003, pp. 1387-1394.

[3] K. Tan, J. P. Oakley, Enhancement of Color Images in Poor Visibility Conditions, *Proceedings of IEEE International Conference on Image Processing*, Vancouver, BC, Canada, 2000, pp. 788-791.

[4] S. G. Narasimhan, S. K. Nayar, Contrast Restoration of Weather Degraded Images, *IEEE Transactions on Pattern Analysis and Machine Intelligence*, Vol. 25, No. 6, pp. 713-724, June, 2003.

[5] S. G. Narasimhan, S. K. Nayar, Removing Weather Effects from Monochrome Images, *Proceedings of the 2001 IEEE Computer Society Conference on Computer Vision and Pattern Recognition*, Kauai, HI, USA, 2001, pp. 186-193.

[6] Y. Y. Schechner, S. G. Narasimhan, S. K. Nayar, Polarization-based Vision through Haze, *Applied Optics*, Vol. 42, No. 3, pp. 511-525, January, 2003.

[7] R. Tan, Visibility in Bad Weather from a Single Image, *2008 IEEE Conference on Computer Vision and Pattern Recognition*, Anchorage, AK, USA, 2008, pp. 1-8.

[8] R. Fattal, Single Image Dehazing, *ACM Transactions on Graphics*, Vol. 27, No. 3, pp. 1-9, August, 2008.

[9] K. M. He, J. Sun, X. Tang, Single Image Haze Removal using Dark Channel Prior, *IEEE Transactions on Pattern Analysis and Machine Intelligence*, Vol. 33, No. 12, pp. 2341-2353, December, 2011.

[10] G. F. Meng, Y. Wang, J. Duan, S. Xiang, C. Pan, Efficient Image Dehazing with Boundary Constraint and Contextual Regularization, *Proceedings of the IEEE International Conference on Computer Vision*, Sydney, NSW, Australia, 2013, pp. 617-624.

[11] S. C. Huang, B. H. Chen, W. J. Wang, Visibility Restoration of Single Hazy Images Captured in Real-World Weather Conditions, *IEEE Transactions on Circuits and Systems for Video Technology*, Vol. 24, No. 10, pp. 1814-1824, October, 2014.

[12] D. Berman, T. Treibitz, S. Avidan, Non-local Image Dehazing, *Proceedings of IEEE Conference on Computer Vision and Pattern Recognition*, Las Vegas, NV, USA, 2016, pp. 1674-1682.

[13] K. Tang, J. Yang, J. Wang, Investigating Haze-Relevant Features in a Learning Framework for Image Dehazing, *Proceedings of IEEE Conference on Computer Vision and Pattern Recognition*, Columbus, OH, USA, 2014, pp. 2995-3000.

[14] B. Cai, X. Xu, K. Jia, C. Qing, D. Tao, Dehazenet: An End-to-End System for Single Image Haze Removal, *IEEE Transactions on Image Processing*, Vol. 25, No. 11, pp. 5187-5198, November, 2016.

[15] M. Zhu, B. He, Q. Wu, Single Image Dehazing Based on Dark Channel Prior and Energy Minimization, *IEEE Signal Processing Letters*, Vol. 25, No. 2, pp. 174-178, February, 2018.

[16] J. S. Lee, C. H. Li, H. Y. Lee, Visibility Dehazing based on Channel-Weighted Analysis and Illumination Tuning, *Multimedia Tools and Applications*, Vol. 78, No. 2, pp. 1831-1856, January, 2019.

[17] Y. T. Peng, K. Cao, P. C. Cosman, Generalization of the Dark Channel Prior for Single Image Restoration, *IEEE Transactions on Image Processing*, Vol. 27, No. 6, pp. 2856-2868, June, 2018.

[18] G. Bi, J. Ren, T. Fu, T. Nie, C. Chen, N. Zhang, Image Dehazing Based on Accurate Estimation of Transmission in the Atmospheric Scattering Model, *IEEE Photonics Journal*, Vol. 9, No. 4, pp. 1-18, August, 2017.

[19] J. M. Guo, J. Y. Syue, V. R. Radzicki, H. Lee, An Efficient Fusion-based Defogging, *IEEE Transactions on Image Processing*, Vol. 26, No. 9, pp. 4217-4228, September, 2017.

[20] X. Liu, H. Zhang, Y. Y. Tang, J. X. Du, Scene-Adaptive Single Image Dehazing via Opening Dark Channel Model, *IET Image Processing*, Vol. 10, No. 11, pp. 877-884, November, 2016.

[21] Y. Liu, H. Li, M. Wang, Single Image Dehazing via Large Sky Region Segmentation and Multiscale Opening Dark Channel Model, *IEEE Access*, Vol. 5, pp. 8890-8903, May, 2017.

[22] K. He, J. Sun, X. Tang, Guided Image Filtering, *IEEE Transactions on Pattern Analysis and Machine Intelligence*, Vol. 35, No. 6, pp. 1397-1409, June, 2013.

[23] W. Niblack, An Introduction to Digital Image Processing, *Prentice-Hall*, 1986.

[24] H. Jegou, M. Douze, C. Schmid, Hamming Embedding and Weak Geometric Consistency for Large Scale Image Search, *Proceedings of the 10th European Conference on Computer*, Marseille, France, 2008, pp. 304-317.

[25] J. Shin, M. Kim, J. Paik, S. Lee, Radiance-Reflectance Combined Optimization and Structure-Guided ℓ_0-Norm for Single Image Dehazing, *IEEE Transactions on Multimedia*, Vol. 22, No. 1, pp. 30-44, January, 2020.

Biographies

Jung-San Lee has worked as a professor in the Department of Information Engineering and Computer Science at Feng Chia University, Taichung, Taiwan. His current research interests include image processing, information security, and watermarking.

Yun-Yi Fan is pursuing her PhD degree in information engineering and computer science in Feng Chia University, Taichung, Taiwan. Her current research interests include image processing and blockchain applications.

Hsin-Yu Lee received MS degree in information engineering and computer science in Feng Chia University, Taichung, Taiwan in 2019. Her current research interests include image processing and information security.

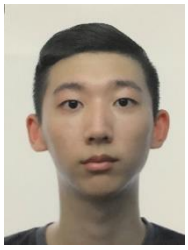

Gah Wee Yong is pursuing his MS degree in information engineering and computer science in Feng Chia University, Taichung, Taiwan. His current research interests include image processing and network security.

Ying-Chin Chen is pursuing her PhD degree in information engineering and computer science in Feng Chia University, Taichung, Taiwan. Her current research interests include information security and visual secret sharing.